Earth and Planetary Science Letters 362 (2013) 207–214

Contents lists available at SciVerse ScienceDirect

Earth and Planetary Science Letters

journal homepage: www.elsevier.com/locate/epsl

# Constraints of the topography, gravity and volcanism on Venusian mantle dynamics and generation of plate tectonics

Jinshui Huang [a,*], An Yang [a], Shijie Zhong [b]

[a] Mengcheng National Geophysical Observatory, School of Earth and Space Science, University of Science and Technology of China, Hefei 230026, China
[b] Department of Physics, University of Colorado at Boulder, Boulder, CO 80309, USA

ARTICLE INFO

*Article history:*
Received 4 September 2012
Received in revised form
22 November 2012
Accepted 27 November 2012
Editor: T. Spohn

*Keywords:*
plate tectonics
Venusian mantle dynamics
volcanism
geoid
topography
admittance

ABSTRACT

Venus's mantle convection model was studied in a three-dimensional spherical shell domain with depth- and temperature-dependent viscosity. Numerical results show that key observations of Venus including the number of major "hotspot" volcanic systems, spectral patterns of the surface topography and geoid at long- and intermediate-wavelengths can be explained in models that have a spinel-to-post-spinel endothermic phase change of $-3.5$ MPa/K Clapeyron slope and averaged mantle viscosity of $2 \times 10^{21}$ Pa s (i.e., convective Rayleigh number of $1.8 \times 10^{7}$). Our models with the endothermic phase change show relatively weak time-dependence, suggesting that the phase change may not be the primary cause for "catastrophic" resurfacing on Venus. Our calculations also show that Venus cannot have a weak asthenosphere that is similar to that on the Earth, in order to match the observations, thus supporting a key role of asthenosphere in producing plate tectonics.



## 1. Introduction

Despite of their similar sizes and compositions, Venus and the Earth show distinctly different surface tectonics and dynamic evolution. Venus is characterized by one-plate, stagnant-lid mantle convection, while the Earth is controlled by mobile-lid, plate tectonics type of convection (Kaula and Phillips, 1981; Nimmo and Mckenzie, 1998; Smrekar et al., 2007). What controls the style of mantle convection, i.e., stagnant-lid versus plate tectonic convection, remains one of the most important unresolved questions in geodynamics. While lithospheric deformation including faulting plays important roles (Moresi and Solomatov, 1998; O'Neill et al., 2007), recent studies suggest that weak asthenosphere also exerts a significant control on generation of plate tectonics (Höink et al., 2012; Richards et al., 2001).

Venus is a geologically active planet with significant young volcanism, as observed recently by the Venus Express spacecraft (Smrekar et al., 2010). These surface features of volcanism and tectonics, together with satellite observations of surface topography and gravity anomalies by the Pioneer Venus Orbiter and Megellan spacecraft (Konopliv et al., 1999; Konopliv and Sjogren, 1994; Rappaport et al., 1999; Sjogren et al., 1997), provide important constraints on the dynamics of Venus. The gravity and topography anomalies on Venus are highly correlated and show a relatively large ratio or admittance at lower degrees (Fig. 1), suggesting a dynamic origin for these anomalies (Pauer et al., 2006; Simons et al., 1997; Smrekar and Phillips, 1991). Mantle dynamic modeling of large topographic rises with volcanic features showed that their gravity and topography can be explained as a result of mantle upwelling plumes (Kiefer and Hager, 1991; Nimmo and McKenzie, 1996; Smrekar and Parmentier, 1996). Such features are known as "hotspot" on Earth, with Hawaii being the classic example. Nine "hotspots" have been identified based on observations of geologic features, gravity anomalies and topographic rises, and several of them are supposed to be with geologically recent volcanism based on recent data from Venus Express (Smrekar et al., 2010; Stofan et al., 1995). Therefore, these nine "hotspots" or mantle plumes represent the characteristic convective wavelength for Venus (Smrekar and Sotin, 2012).

However, little effort has been made to investigate the relationship between the spectra of the topography and gravity and mantle convective structure in global models of stagnant-lid mantle convection. Such studies are necessary for two reasons. First, the topography and gravity spectra are inherently related to mantle convective structure at intermediate- and long-wavelengths. While convective structure wavelength is often prescribed in regional models for individual plumes, only global models of mantle convection yield dynamically self-consistent convective structure (e.g., the number of plumes). Second, convective structure including its dominant wavelength is affected significantly by

* Corresponding author. Tel./fax: +86 551 3606781.
*E-mail address:* jshhuang@ustc.edu.cn (J. Huang).

0012-821X/$ - see front matter © 2012 Elsevier B.V. All rights reserved.
http://dx.doi.org/10.1016/j.epsl.2012.11.051

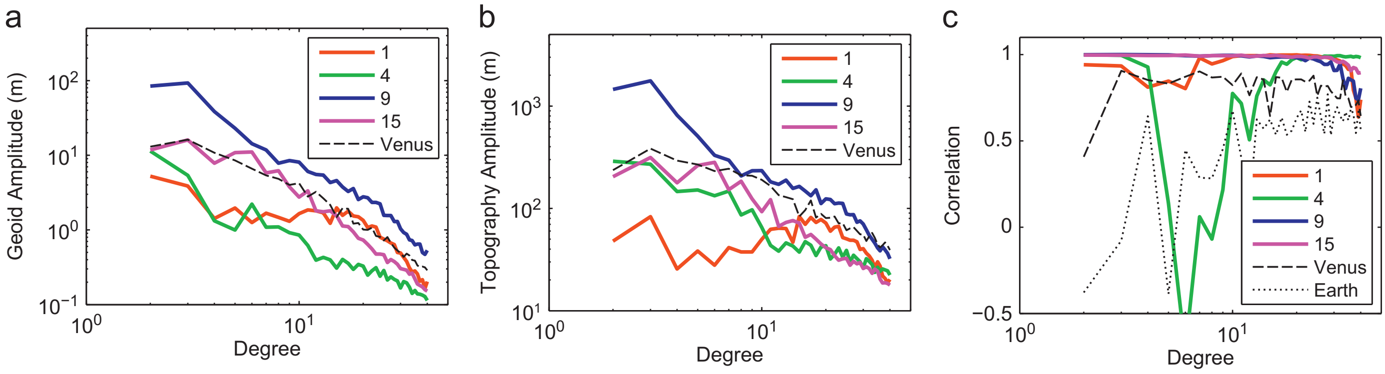


**Fig. 1.** Power spectra of geoid (a), topography (b), and correlation between geoid and topography (c) for Venus and Cases 1, 4, 9 and 15. Also included in (c) are results for the Earth.

mantle viscosity structure and mantle phase changes (Roberts and Zhong, 2006; Tackley, 1996). For example, stagnant-lid convection with relatively uniform mantle viscosity under the lid that is preferred by regional models of individual plumes (Kiefer and Hager, 1991), typically contains a large number of mantle plumes (Reese et al., 1999; Smrekar and Sotin, 2012) that may be inconsistent with the inferred nine mantle plumes for Venus. However, both endothermic spinel-to-post-spinel phase change and asthenosphere may increase the dominant convective wavelength and reduce the number of plumes (Roberts and Zhong, 2006).

We have formulated three-dimensional global models of mantle convection to simultaneously explain the number of plumes and the spectra of surface topography and gravity (i.e., geoid) for Venus. The models employ the extended-Boussinesq approximation and realistic temperature- and depth-dependent viscosity, similar to those used for Mars (Roberts and Zhong, 2006). In total, 15 cases are computed. By comparing with observations we seek constraints on mantle dynamics including the mantle viscosity structure, convective vigor, and phase changes.

## 2. Model setup

The Venus' mantle is treated as an infinite Prandtl number fluid in a three dimensional spherical shell under the extended Boussinesq approximation. The non-dimensional governing equations of mantle convection are (Zhong, 2006; Zhong et al., 2008):

$$\nabla\cdot\mathbf{u}=0 \tag{1}$$

$$-\nabla P+\nabla\cdot[\eta(\nabla\mathbf{u}+\nabla^T\mathbf{u})]+\left(\frac{R_0}{D}\right)^3\left[RaT-\sum_{k=1}^{2}(Ra_k\Gamma_k)\right]\mathbf{e}_r=0 \tag{2}$$

$$\left(\frac{\partial T}{\partial t}+\mathbf{u}\cdot\nabla T\right)\left[1+\sum_{k=1}^{2}\left(\gamma_k^2\frac{Ra_k}{Ra}\frac{d\Gamma_k}{d\pi_k}\right)D_i(T+T_s)\right]=\nabla^2T$$
$$-\left(1+\sum_{k=1}^{2}\gamma_k\frac{Ra_k}{Ra}\frac{d\Gamma_k}{d\pi_k}\right)D_i(T+T_s)u_r+\left(\frac{D}{R_0}\right)^3\frac{D_i}{Ra}\sigma_{ij}\frac{\partial u_i}{\partial x_j}+H \tag{3}$$

where $\mathbf{u}$, $P$, $\eta$, $T$, $T_s$, $D_i$, $u_r$, $\sigma_{ij}$ and $H$ are the velocity vector, pressure, viscosity, temperature, surface temperature, dissipation number, radial velocity, deviatoric stress, and heat production rate, respectively. $R_0$ is the radius of Venus and $D$ is the Venusian mantle thickness. $\Gamma_k$, $\gamma_k$, and $\pi_k$ are phase function, Clapeyron slope, and excess pressure for phase $k$ ($k$=1 and 2 for olivine–spinel and spinel–perovskite phase changes, respectively), respectively (Christensen and Yuen, 1985). $\mathbf{e}_r$ is the unit vector in radial direction. $Ra$ and $Ra_k$ are a Rayleigh number and phase change Rayleigh number for phase change $k$ ($k$=1 and 2), respectively. Characteristic scales for the above equations are: length $R_0$, time $R_0^2/\kappa$ ($\kappa$ is the thermal diffusivity), and temperature $\Delta T$. $Ra$, $Ra_k$, $D_i$ and $H$ are defined as

$$Ra=\frac{\rho_0 g\alpha\Delta TD^3}{\kappa\eta_0} \tag{4}$$

$$Ra_k=\frac{\delta\rho_k}{\rho_0\alpha\Delta T}Ra \tag{5}$$

$$D_i=\alpha gR_0/C_p \tag{6}$$

$$H=\frac{QR_0^2}{C_p\rho_0\Delta T\kappa} \tag{7}$$

where $\rho_0$ and $\eta_0$ are the reference values for density and viscosity. $\alpha$, $g$ and $C_p$ are coefficient of thermal expansion, gravitational acceleration and specific heat, respectively. $\delta\rho_k$ is the density change for phase change $k$ ($k$=1 and 2) and $Q$ is the volumetric internal heat generation rate.

The viscosity of the mantle is assumed to be temperature- and pressure-dependent (Karato and Jung, 2003). The non-dimensional viscosity in our model is given by

$$\eta=\eta_r\exp\left[\frac{E+V(1-r)}{T+T_s}-\frac{E+V(1-r_{core})}{1+T_s}\right] \tag{8}$$

where $\eta_r$ is a pre-exponential factor, which is used to specify the viscosity contrast between the upper and lower mantle, and $\eta_r$ is reduced for the upper mantle (*i.e.*, above the 690 km depth) to model the weak asthenosphere. $r$ is the non-dimensional radial position, $r_{core}$ is the Venusian non-dimensional core radius, and $E$ and $V$ are the non-dimensional values of activation energy, $E^*$, and activation volume, $V^*$, which are given by

$$E=\frac{E^*}{R\Delta T},V=\frac{\rho_0 gDV^*}{R\Delta T} \tag{9}$$

where $R$ is the gas constant. The viscosity is cut off with a maximum non-dimensional value of $2\times10^4$ at the surface. Table 1 lists model parameter values.

Among the model parameters, we mainly consider three controlling parameters in our models, i.e., Rayleigh number, $Ra$, viscosity pre-factor, $\eta_r$, and Clapeyron slope of the phase changes, $\gamma$, with the goal to search and find these parameters that could reproduce the observations on Venus. With less constraint for Venus, most of the parameters used here are based on those for the Earth. The viscosity in the Earth's mantle is on average $\sim10^{21}-10^{22}$ Pa s with the lower mantle that may be a factor of 30 stronger than the upper mantle (e.g. Hager and Richards, 1989). Therefore, in our models here to test the influences of a weak upper mantle (or asthenosphere), the upper mantle viscosity is set to be 3–30 times weaker

**Table 1**
Model parameter values.

| Parameter | Value |
|---|---|
| Venusian radius $R_0$ | 6050 km |
| Inner radius $r_{core}$ | 3330 km |
| Surface temperature $T_s$ | 730 K |
| Temperature difference $\Delta T$ | 2500 K |
| Reference density $\rho_0$ | 3300 kg/m$^3$ |
| Specific heat $C_p$ | 1200 J/(K kg) |
| Thermal diffusivity $\kappa$ | $8.1 \times 10^{-7}$ m$^2$/s |
| Thermal expansivity $\alpha$ | $2 \times 10^{-5}$/K |
| Activation energy $E^*$ | 150 kJ/mol |
| Activation volume $V^*$ | 1.5 cm$^3$/mol |
| Dissipation number $D_i$ | 0.89 |
| Gravitational acceleration $g$ | 8.87 m/s$^2$ |
| Olivine-spinel phase change ($k=1$) | |
| Position | 490 km |
| Half-width | 50 km |
| Density change $\delta\rho_1$ | 210 kg/m$^3$ |
| Spinel-perovskite phase change ($k=2$) | |
| Position | 690 km |
| Half-width | 50 km |
| Density change $\delta\rho_2$ | 210 kg/m$^3$ |

through varying $\eta_r$. We vary $Ra$ to take into account the range of possible mantle averaged viscosity. The Clapeyron slope of phase changes is set to vary from $\pm 3$ to $\pm 5$ MPa/K in our model (e.g. Christensen and Yuen, 1985).

However, we used relatively small activation energy and activation volume and did not vary them in our models. The relatively small activation energy was used because we used a Newtonian rheology to approximate a non-Newtonian rheology (Christensen, 1984; Karato and Wu, 1993; van Hunen et al., 2005). The reduced activation volume is mainly for relatively small depth-dependence of viscosity, to keep the models simple. We also point out that depth-dependent viscosity is also introduced in the pre-factor of viscosity equation at the upper–lower mantle boundary. We also varied internal heat generation in the models to maintain a relatively large internal heating ratio ($\sim$80%) for Venus mantle convection. Large internal heating ratio or small CMB heat flux may be required for Venus because of the lack of an active dynamo. For this reason, in this study we only consider models with similarly large internal heating ratios. The dimensional internal heat generation considered here is between $2 \times 10^{-12}$ W/kg and $6 \times 10^{-12}$ W/kg, which is compatible with the current Earth and also with a recent study on Venus' mantle convection (Smrekar and Sotin, 2012). Our calculations are performed with the 3-D spherical finite element and parallel code CitcomS (Zhong et al., 2008). The spherical shell is divided into 12 approximately equal size caps and each cap is further divided into either $48^3$ or $64^3$ elements, depending on convective vigor. Radial resolution is doubled for the top and bottom thermal boundary layers such that there are at least three elements to cover each of the boundary layers. Our resolution tests show that the resolution is sufficient to resolve the heat flux across the boundary layers.

For all the calculations, we use free-slip boundary conditions for the surface and the bottom boundary. We run a test case to obtain its horizontally averaged temperature, and use it as initial temperature for all cases. All cases are run until convective heat fluxes are in a quasi-steady state. Table 2 lists all the 15 cases performed for this study. For each case, we compute its averaged surface and bottom heat flux ($q_s$ and $q_b$), averaged temperature and root-mean-square velocity of the whole mantle for each time step. Internal heating ratio is computed as $(q_s - q_b)/q_s$. Because these values change with time in quasi-steady state convection, we compute their time averages over the final 4000 time steps of each model, which are also list in Table 2 as averaged surface heat flux $Q_s$, averaged mantle temperature $\langle T \rangle$, averaged internal heating ratio $f_H$, and averaged mantle root-mean-square velocity $V_{rms}$, respectively. Lithospheric thickness $\delta$, also listed in Table 2, is computed based on horizontally averaged viscosity and is defined as the thickness of the layer in the upper thermal boundary with a viscosity 10 times larger than the average viscosity of the upper mantle below the lithosphere.

## 3. Numerical results

We quantify dynamic topography, geoid and number of upwelling plumes from our models. Dynamic topography and geoid anomalies are computed using a formulation that includes the self-gravitation and employs consistent boundary flux techniques (Leng and Zhong, 2008). Dynamic topography includes contributions only from mantle dynamics with no contribution from the crust buoyancy (Hager and Richards, 1989). The number of plumes is determined using the similar method in Leng and Zhong (2008) (also see Smrekar and Sotin, 2012) that is outlined as follows. For a given time frame, we use the temperature field in the upper mantle at the 425-km depth to identify upwelling plumes. Define a threshold temperature $T_c = T_{ave} + f(T_{max} - T_{ave})$, where $T_{ave}$ and $T_{max}$ are the average and maximum temperature at the 425-km depth, and $f$ is chosen to be 0.2. Only a plume with its center temperature greater than $T_c$ and its plume heat flux greater than 5% of the maximum plume heat flux is counted. The choices of parameter $f$ and the 5% plume heat flux threshold do not affect results significantly (Leng and Zhong, 2008). Because the number of plumes changes with time, we compute an average, $N_{plume}$, for the final 4000 time steps of a model. A standard deviation for $N_{plume}$ is also determined and the time variability of the number of plumes is measured (Table 2).

Case 1 includes temperature- and pressure-dependent viscosity with a unit pre-exponential factor (i.e., no asthenosphere), Rayleigh number $Ra = 7.3 \times 10^6$, and no phase changes (Table 2). The horizontally averaged temperature and viscosity indicate $\sim$240 km thick top thermal boundary layer or lithosphere with a viscosity that is five orders of magnitude larger than the mantle below (Fig. 2), characterizing a stagnant-lid convection. The pressure-dependent viscosity leads to six times of gradual increase in viscosity with depth from the base of lithosphere to the core–mantle boundary (CMB) region. The time-averaged internal heating ratio is 78% (Table 2), suggesting largely internally heated convection with small heat flux at the CMB. A representative convective thermal structure (Fig. 3a) shows dominant short-wavelengths with 78 upwelling plumes (Table 2), typical of stagnant-lid convection (Orth and Solomatov, 2011; Smrekar and Sotin, 2012; Zhong et al., 2008). While the surface topography and geoid are highly correlated (Figs. 1c and 3a), the powers of topography and geoid spectra are significantly reduced at long-wavelengths, compared with the observed (Fig. 1a and b).

Cases 2–4 differ from Case 1 in having an asthenosphere that is realized by reducing the pre-exponential factor of the viscosity equation for the upper mantle by a factor of 3, 10 and 30, respectively (Fig. 2b and Table 2). Because the asthenosphere leads to more vigorous convection and larger surface heat flux, internal heat generation rates are increased to maintain similarly large internal heating ratios (Table 2). Cases 2, 3 and 4 have on average 19, 12 and 10 plumes, respectively, compared with 78 plumes in Case 1 (Table 2), reflecting the effect of asthenosphere on promoting long-wavelength convective structures (Roberts and Zhong, 2006). The increased convective wavelengths for Cases 2–4 are also evident in the thermal structure, surface topography and geoid (Figs. 1 and 3b for Case 4 and Figs. 4 and 5a). However, the powers of topography and geoid for Cases 2–4

**Table 2**
Model input parameters and outputs.

| Case no. | $Ra$ | $H$ | $1/\eta_r$ | $\gamma$ (MPa/K) | $\langle T \rangle$ | $Q_s$ | $f_H$ (%) | $N_{plume}$[a] | $V_{rms}$ | $\delta$ (km) |
|---|---|---|---|---|---|---|---|---|---|---|
| 1 | $7.3\times10^6$ | 30 | 1 | No | 0.618 | 10.1 | 78.0 | 78.1($\pm$17.6) | 698.5 | 245 |
| 2 | $7.3\times10^6$ | 40 | 3 | No | 0.621 | 12.9 | 80.8 | 19.2($\pm$5.0) | 1258 | 182 |
| 3 | $7.3\times10^6$ | 60 | 10 | No | 0.613 | 17.3 | 82.0 | 11.7($\pm$2.5) | 2231 | 134 |
| 4 | $7.3\times10^6$ | 90 | 30 | No | 0.596 | 23.2 | 82.3 | 9.9($\pm$0.3) | 3656 | 103 |
| 5 | $3.7\times10^6$ | 45 | 10 | No | 0.607 | 14.0 | 81.1 | 14.6($\pm$3.3) | 1290 | 167 |
| 6 | $1.5\times10^7$ | 75 | 10 | No | 0.607 | 20.9 | 80.0 | 9.1($\pm$2.3) | 3599 | 109 |
| 7 | $7.3\times10^6$ | 30 | 1 | $\pm$3 | 0.617 | 10.5 | 73.2 | 76.2($\pm$4.4) | 702.5 | 236 |
| 8 | $7.3\times10^6$ | 30 | 1 | $\pm$4 | 0.637 | 10.6 | 72.4 | 24.4($\pm$4.7) | 718.6 | 245 |
| 9 | $7.3\times10^6$ | 30 | 1 | $\pm$5 | 0.646 | 9.72 | 79.5 | 3.1($\pm$0.3) | 584.7 | 270 |
| 10 | $1.8\times10^7$ | 40 | 1 | $\pm$3 | 0.636 | 13.1 | 75.5 | 14.6($\pm$3.8) | 1353 | 197 |
| 11 | $2.7\times10^7$ | 45 | 1 | $\pm$3 | 0.637 | 14.6 | 75.2 | 11.7($\pm$3.0) | 1777 | 176 |
| 12 | $3.6\times10^7$ | 45 | 1 | $\pm$3 | 0.629 | 15.1 | 72.0 | 9.8($\pm$3.9) | 2098 | 170 |
| 13 | $1.8\times10^7$ | 40 | 1 | $\pm$4 | 0.648 | 12.7 | 74.4 | 3.0($\pm$1.1) | 1259 | 212 |
| 14 | $3.6\times10^7$ | 45 | 1 | $\pm$4 | 0.634 | 15.2 | 69.9 | 3.3($\pm$0.5) | 1886 | 203 |
| 15 | $1.8\times10^7$ | 40 | 1 | $\pm$3.5 | 0.643 | 13.1 | 75.4 | 7.8($\pm$3.4) | 1356 | 200 |

[a] The numbers in parentheses are the standard deviations.

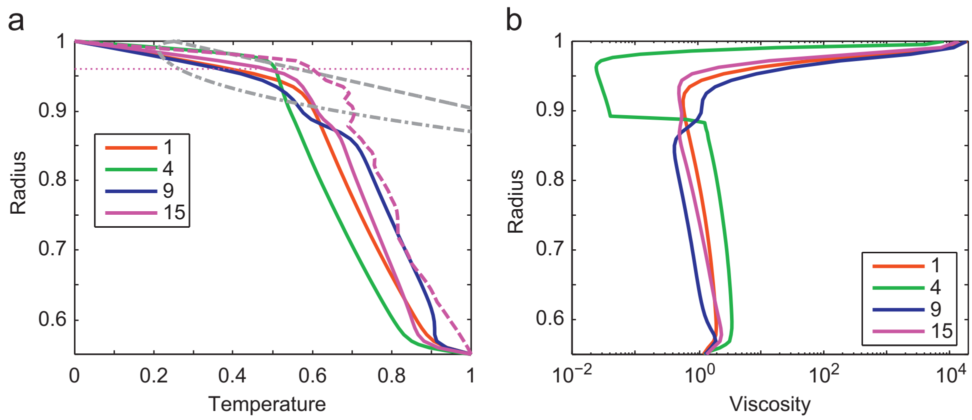


**Fig. 2.** Radial dependence of horizontally averaged non-dimensional temperature (a) and viscosity (b) for Cases 1, 4, 9 and 15. In (a), the gray lines represent melting curves for dry peridotite (dashed line) and wet peridotite (dash-dotted line), and the magenta dashed curve and the dotted line are for the maximum temperature at different depths (i.e., within the plumes) and the bottom of thermal lithosphere in Case 15, respectively. (For interpretation of the references to color in this figure legend, the reader is referred to the web version of this article.)

remain significantly less than the observed (Fig. 1a and b). In particular, the negative correlations for Case 4 between spherical harmonic degrees $l=5$–9 indicate positive (negative) geoid anomalies over topographic lows (highs), which is characteristic of Earth's mantle convection with a weak asthenosphere (Hager and Richards, 1989), but inconsistent with Venus. Since Case 2 has significantly more plumes than the observed, this leaves Case 3 with a factor of 10 viscosity reduction in the upper mantle as more viable. However, additional calculations of Cases 5 and 6 that differ from Case 3 in having different $Ra$ show that the powers of topography and geoid for these cases are always significantly smaller than the observed (Fig. 4).

We now present models with olivine-to-spinel exothermic and spinel-to-post-spinel endothermic phase changes that should exist in Venus at depths of 490 km and 690 km, respectively (Schubert et al., 1997; Steinbach and Yuen, 1992). An endothermic phase change is known to promote long-wavelength convective structures (Tackley et al., 1993, 1994). Such effects of the endothermic phase change depend on $Ra$ and Clapeyron slope, and are stronger for larger $Ra$ and Clapeyron slope (Christensen and Yuen, 1985; Tackley et al., 1993, 1994). Cases 7, 8 and 9 include these phase changes with Clapeyron slopes $\gamma$ of $\pm 3$, $\pm 4$, and $\pm 5$ MPa/K, respectively, but these cases are otherwise identical to Case 1 (Table 2). That is, these cases also include a stagnant-lid and strongly temperature-dependent viscosity that were not included in a previous global mantle convection model with the phase changes for Venus (Schubert et al., 1997). Here we assume that the two phase changes have the same magnitude of Clapeyron slopes. However, the dynamics is mainly controlled by the endothermic phase change (Zhong and Gurnis, 1994). The dominant convective wavelength increases and the number of plumes decreases with the magnitude of Clapeyron slopes $|\gamma|$ (Figs. 5b and 3c for Cases 8 and 9, respectively). The number of plumes is 76, 24 and 3, as $|\gamma|$ increases from 3, 4 to 5 MPa/K for Cases 7, 8 and 9, respectively (Table 2). The powers of the topography and geoid spectra also increase with $|\gamma|$ (Fig. 6). Case 8 with $|\gamma|=4$ MPa/K provides the best fit to the observed spectra among these three cases (Fig. 6), but with 24 plumes this case significantly over-predicts the number of plumes.

Cases 10, 11 and 12 with the same $|\gamma|=3$ MPa/K as Case 7 but higher $Ra$ at $1.8\times10^7$, $2.7\times10^7$ and $3.6\times10^7$, respectively, explore the effects of $Ra$. Internal heat generation rate for Cases 10–12 is increased accordingly to maintain similar internal heating ratios (Table 2). Cases 10–12 show that for a given Clapeyron slope $|\gamma|$, increasing $Ra$ leads to increase in convective wavelengths. The number of plumes decreases to 15, 12 and 10 for Cases 10, 11 to 12, respectively (Table 2). Consequently, the

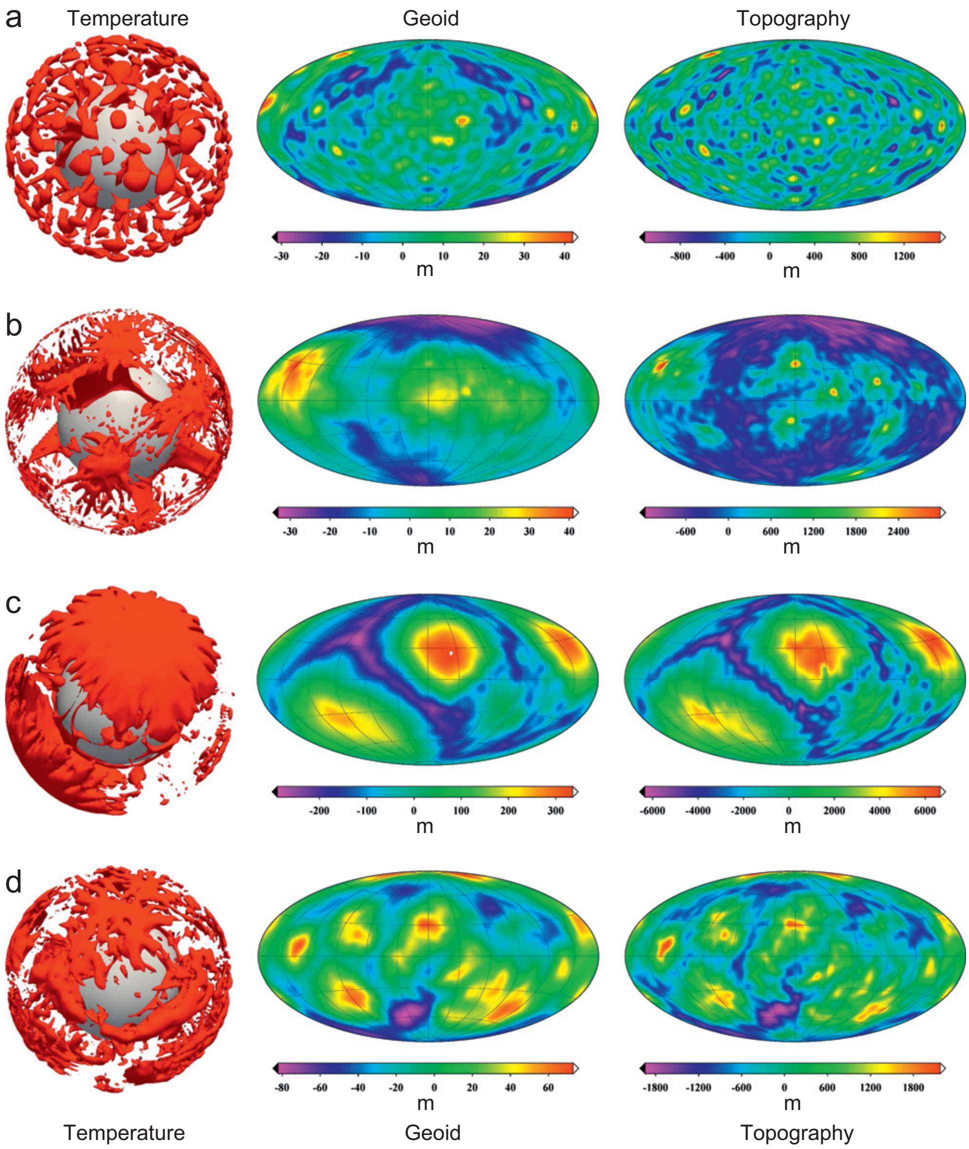


**Fig. 3.** Representative thermal structures represented by residual temperature iso-surfaces of upwelling plumes (left column), geoid (middle column) and surface topography (right column) for Cases 1 (a, first row), 4 (b, second row), 9 (c, third row) and 15 (d, bottom row), respectively. Iso-surfaces of residual temperature have a non-dimensional value of 0.03.

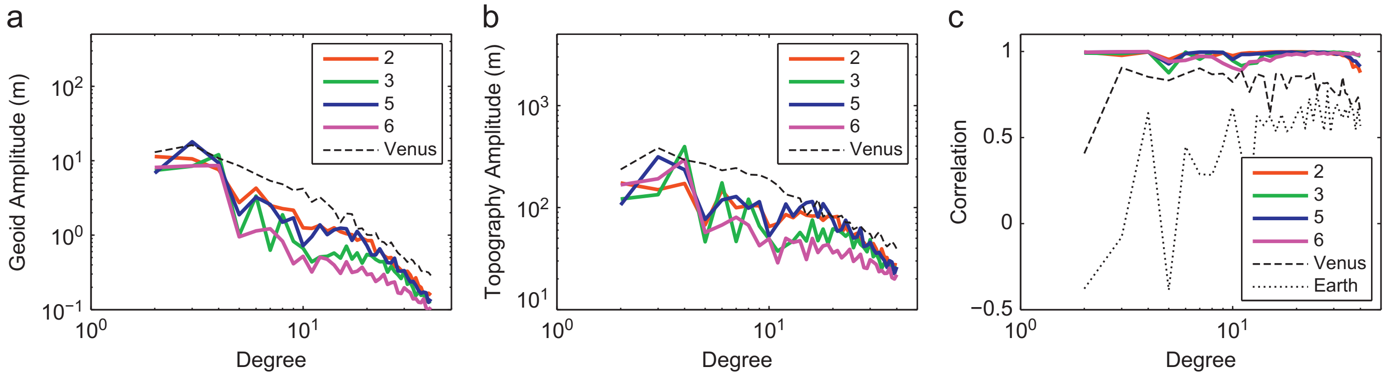


**Fig. 4.** Power spectra of geoid (a), topography (b), and correlation between geoid and topography (c) for Venus and Cases 2, 3, 5 and 6. Also included in (c) are results for the Earth.

power spectra of the topography and geoid increase at relatively long wavelengths as $Ra$ increases (Fig. 7). The results from these six phase change calculations (Cases 7–12) are further confirmed by Cases 13–15 with varying $Ra$ and Clapeyron slopes (Table 2). In particular, Case 15 with Clapeyron slopes of $\pm 3.5$ MPa/K and $Ra = 1.8 \times 10^7$ (i.e., averaged mantle viscosity of $2 \times 10^{21}$ Pa s, if

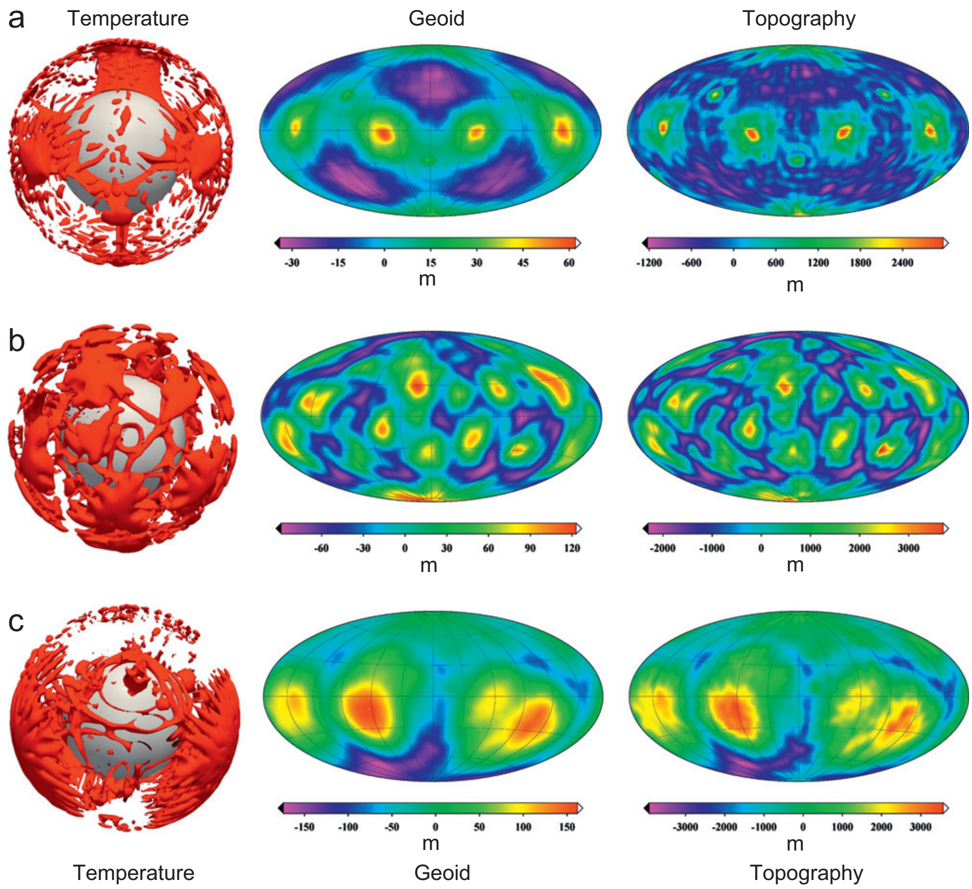


**Fig. 5.** Representative thermal structures represented by residual temperature iso-surfaces of upwelling plumes (left column), geoid (middle column) and surface topography (right column) for Cases 3 (a, first row), 8 (b, second row) and 13 (c, third row), respectively. Iso-surfaces of residual temperature have a value of 0.03.

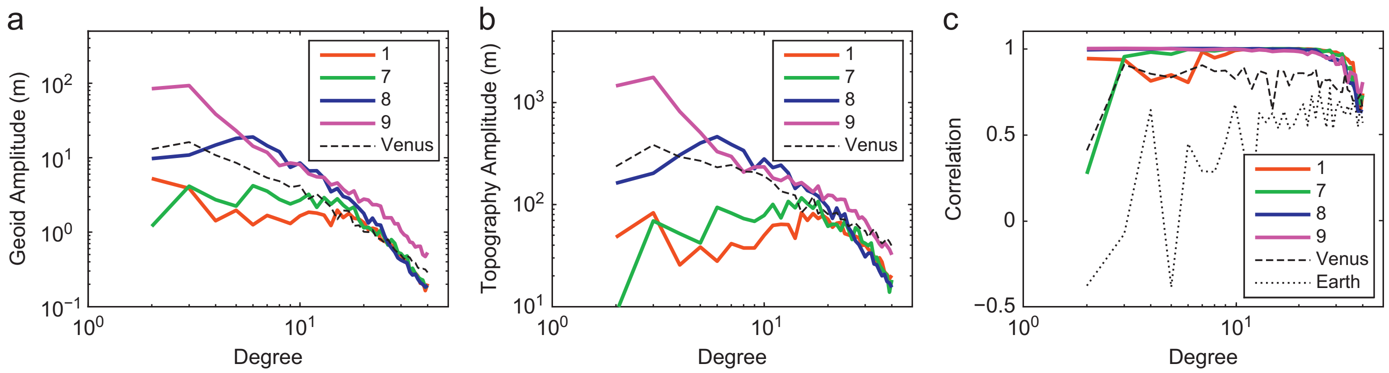


**Fig. 6.** Power spectra of geoid (a), topography (b), and correlation between geoid and topography (c) for Venus and Cases 1, 7, 8 and 9. Also included in (c) are results for the Earth.

scaled using parameters in Table 1) reproduces the number of plumes and the topography and geoid spectra the best (Figs. 1 and 3d and Table 2). All the cases with phase changes show positively correlated topography and geoid, consistent with the observed (Figs. 1, 6 and 7).

Our results show that phase changes may affect convective wavelengths and hence the number of plumes significantly (e.g. Tackley et al., 1993). It should be pointed out that phase changes may lead to different numbers of plumes in the upper and lower mantles. For example, Fig. 8 shows a zoom-in view of plume structures for case 15. Under each large plume in the upper mantle, there are several small separate plumes in the lower mantle.

## 4. Discussions

Our models represent the first three-dimensional spherical mantle convection calculations for Venus with realistic temperature- and pressure-dependent viscosity and phase changes, although previous studies considered separately either temperature-dependent viscosity (Orth and Solomatov, 2011) or phase changes (Schubert et al., 1997). We would like to make three remarks relevant to previous mantle convection modeling studies for Venus. (1) The episodic major mantle overturn or mantle “avalanche” associated with the endothermic phase change was suggested to cause the resurfacing of Venus, based on two-dimension models (Steinbach and Yuen, 1992). However, our models with the endothermic phase change show

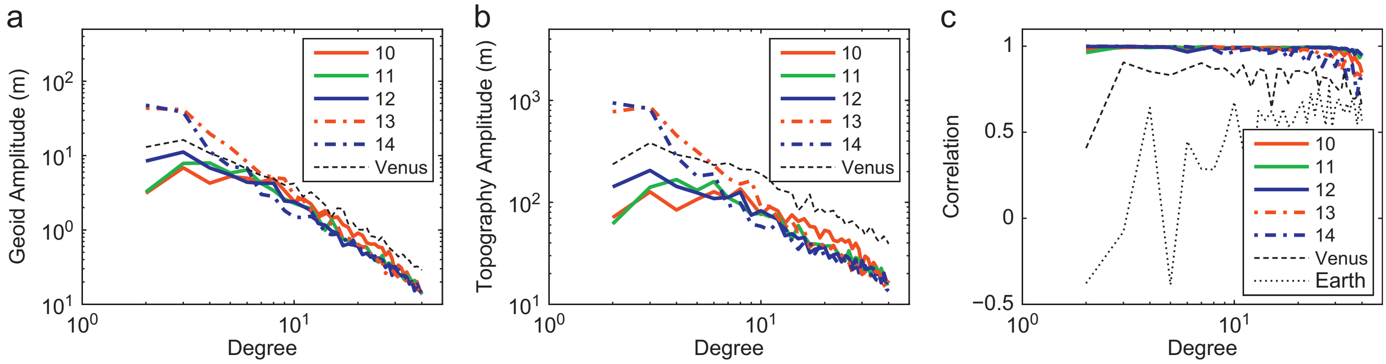


**Fig. 7.** Power spectra of geoid (a), topography (b), and correlation between geoid and topography (c) for Venus and Cases 10–14. Also included in (c) are results for the Earth.

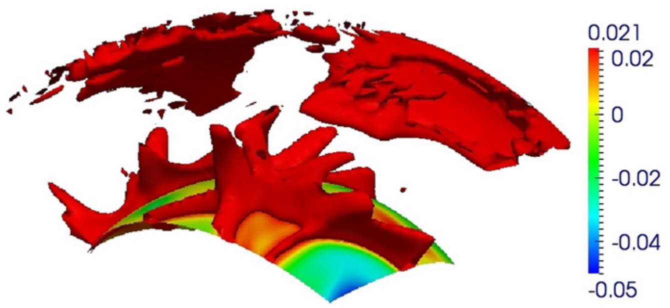


**Fig. 8.** Isosurfaces of residual temperature showing plume structures for Case 15. The isosurface contour is for residual temperature of 0.021, which is the $T_c$ value used for determining the plume number in the upper mantle. Also shown is the residual temperature at the CMB. Note that for clarity, the structure for the top 425 km of the mantle was removed and only a small regional domain ($90^\circ \times 30^\circ$) was shown.

relatively weak time-dependence, due to the combined effects of temperature-dependent viscosity and three-dimensional geometry in our models (Schubert et al., 1997; Zhong and Gurnis, 1994). (2) Stagnant-lid convection can have a variety of different dominant convective wavelengths, ranging from the traditional short-wavelength mushroom-type convection for relatively uniform mantle viscosity (Case 1) to long-wavelength convection when endothermic phase change or weak asthenosphere is present (Fig. 3). (3) Schubert et al. (1997) studied the effects of phase changes on the topography and geoid spectra in global models of mantle convection, but unlike our models their models ignored temperature-dependent viscosity and stagnant-lid convection which may affect convective structure significantly.

The absence of plate tectonics on Venus, a planet with a similar size and composition to the Earth, has prompted a number of proposals on controls for generation of plate tectonics (Kaula and Phillips, 1981; Nimmo and Mckenzie, 1998), and most proposals are related to lithospheric deformation (Landuyt and Bercovici, 2009; Lenardic and Kaula, 1994; Moresi and Solomatov, 1998). Recent studies suggest that weak asthenosphere may play an essential role in generating plate tectonics by increasing lithospheric stress to promote localized lithospheric deformation and by organizing long-wavelength convection (Höink et al., 2012). This proposal is corroborated by our findings and previous studies (Kiefer and Hager, 1991) that reject an Earth-like asthenosphere for Venus. This further raises the question on what causes asthenosphere and the differences in tectonics and climate between Venus and Earth. Water may play an essential role in forming asthenosphere on the Earth (Hirth and Kohlstedt, 1996), suggesting that Venus may be devoid of water in the mantle (Kiefer and Hager, 1991; Nimmo and Mckenzie, 1998) and that volatiles and water play an important role in controlling planetary evolution and plate tectonics (Smrekar et al., 2007).

Given that recent studies show evidence of active volcanism on the Venusian surface (Smrekar et al., 2010), it is interesting to see if our models could predict the pressure release melting. The melting curves for dry and wet peridotite are shown in Fig. 2a. The equations for the melting curves are (Basaltic Volcanism Study Project, 1981; Smrekar and Sotin, 2012)

$$T(\mathrm{K}) = 1350 + 0.1P(\mathrm{MPa}) \quad \text{for dry peridotite}$$

$$T(\mathrm{K}) = 1240 + 49.8/[P(\mathrm{GPa}) + 0.323] \quad \text{for } P < 2.4\ \text{GPa and wet peridotite}$$

$$T(\mathrm{K}) = 1266 - 11.8P(\mathrm{GPa}) + 3.5P^2 \quad \text{for } P > 2.4\ \text{GPa and wet peridotite}$$

The averaged temperatures of our models are always smaller than the dry solidus, but are higher than the wet solidus under the lithosphere (Fig. 2a). However, the maximum mantle temperatures from mantle plumes are very close to that of the dry solidus (e.g., Fig. 2a for Case 15). This suggests that our models may explain the recent "hotspot" volcanism but not wide spread, large-scale volcanism (Smrekar et al., 2010), if the Venus' mantle is devoid of water and volatiles.

## 5. Conclusions

Compared with the observations, our model calculations lead to three conclusions. First, our models, as the first attempt for global convection calculations for Venus with realistic mantle viscosity and phase changes, reproduce all the key observations for Venus including the number of plumes and the spectra of topography and geoid (Fig. 1 and Table 2). The model with Clapeyron slopes $\gamma$ of $\pm 3.5$ MPa/K and averaged mantle viscosity of $2 \times 10^{21}$ Pa s (i.e., $Ra = 1.8 \times 10^7$) (Case 15) provides the best fit to the observations, although other models with $Ra$ ranging from $7.3 \times 10^6$ to $3.6 \times 10^7$ and $|\gamma|$ between 3 and 4 MPa/K (Table 2 and Figs. 6 and 7) may also provide a reasonable fit. All these cases have lithospheric thickness ranging from ~170 km to ~240 km (Table 2), consistent with previous studies (Moore and Schubert, 1995). It should be pointed out that while our preferred model of Case 15 reproduces well the geoid spectra, its topography power remains slightly smaller than the observed. This is expected and reasonable, considering that our models ignore the crust and crustal compensation process that produces the topography but negligible geoid anomalies at intermediate- and long-wavelengths for Venus (Smrekar and Phillips, 1991).

Second, the Venusian mantle may not have a weak asthenosphere as that of the Earth's mantle, because such an asthenosphere leads to negative topography–geoid correlations that are inconsistent with the observed (Case 4 in Fig. 1). This conclusion on mantle viscosity is consistent with previous studies of the topography and geoid from regional mantle plume models for individual plume features (Kiefer and Hager, 1991; Smrekar and Phillips, 1991). Although the topography–geoid correlations are improved in cases with a less pronounced asthenosphere (e.g., Cases 3, 5 and 6 with a factor of 10 reduction in viscosity), the powers of the topography and geoid spectra for these cases are significantly smaller than the observed (Fig. 4). Furthermore, our results show that models with the relatively uniform mantle viscosity under lithosphere (i.e., Cases 1 and 2) as suggested by regional models of individual plumes (Kiefer and Hager, 1991; Smrekar and Phillips, 1991) tend to lead to too many mantle plumes that are inconsistent with the observed. Therefore, our results suggest that in order to explain the observed topography and geoid spectra and the number of mantle plumes, the endothermic phase change must play an important role in Venusian mantle dynamics.

Finally, our models with the endothermic phase change show relatively weak time-dependence in heat transfer across the mantle, significantly different from the 2-D convection models. This suggests that the endothermic phase change may only play a limited role in causing the resurfacing. Our preferred model also predicts that partial melting could occur currently in upwelling plumes for a dry Venusian mantle, thus explaining the recently observed active "hotspot" volcanism on Venus.

## Acknowledgments

The authors are thankful for the careful and constructive reviews by Drs. W. Kiefer and S. Smrekar and financial support by NSFC (91014005, 40774045), US-NSF (EAR-1015669 and 1135382), the Knowledge Innovation Program of the Chinese Academy of Sciences to JH and the CAS/SAFEA International Partnership Program for Creative Research Teams.

## References

Basaltic Volcanism Study Project, 1981. Basaltic Volcanism on the Terrestrial Planets. Pergamon Press, Oxford.

Christensen, U.R., 1984. Convection with pressure- and temperature-dependent non-Newtonian rheology. Geophys. J. R. Astron. Soc. 77, 343–384.

Christensen, U.R., Yuen, D.A., 1985. Layered convection induced by phase transitions. J. Geophys. Res. 90, 10291–10300.

Hager, B.H., Richards, M.A., 1989. Long-wavelength variations in Earth's geoid: physical models and dynamical implications. Philos. Trans. R. Soc. London A 328, 309–327.

Hirth, G., Kohlstedt, D.L., 1996. Water in the oceanic upper mantle: implications for rheology, melt extraction and the evolution of the lithosphere. Earth Planet. Sci. Lett. 144, 93–108.

Höink, T., Lenardic, A., Richards, M.A., 2012. Depth-dependent viscosity and mantle stress amplification: implications for the role of the asthenosphere in maintaining plate tectonics. Geophys. J. Int. 191, 30–41.

Karato, S.I., Jung, H., 2003. Effects of pressure on high-temperature dislocation creep in olivine. Philos. Mag. 83, 401–414.

Karato, S.I., Wu, P., 1993. Rheology of the upper mantle: a synthesis. Science 260, 771–778.

Kaula, W.M., Phillips, R.J., 1981. Quantitative tests for plate-tectonics on Venus. Geophys. Res. Lett. 8, 1187–1190.

Kiefer, W.S., Hager, B.H., 1991. A mantle plume model for the equatorial highlands of Venus. J. Geophys. Res. 96, 20947–20966.

Konopliv, A.S., Banerdt, W.B., Sjogren, W.L., 1999. Venus gravity: 180th degree and order model. Icarus 139, 3–18.

Konopliv, A.S., Sjogren, W.L., 1994. Venus spherical harmonic gravity model to degree-60 and order-60. Icarus 112, 42–54.

Landuyt, W., Bercovici, D., 2009. Variations in planetary convection via the effect of climate on damage. Earth Planet. Sci. Lett. 277, 29–37.

Lenardic, A., Kaula, W.M., 1994. Tectonic plates, D″ thermal structure, and the nature of mantle plumes. J. Geophys. Res. 99, 15697–15708.

Leng, W., Zhong, S., 2008. Controls on plume heat flux and plume excess temperature. J. Geophys. Res. 113, B04408.

Moore, W.B., Schubert, G., 1995. Lithospheric thickness and mantle/lithosphere density contrast beneath Beta Regio, Venus. Geophys. Res. Lett. 22, 429–432.

Moresi, L., Solomatov, V., 1998. Mantle convection with a brittle lithosphere: thoughts on the global tectonic styles of the Earth and Venus. Geophys. J. Int. 133, 669–682.

Nimmo, F., McKenzie, D., 1996. Modelling plume-related uplift, gravity and melting on Venus. Earth Planet. Sci. Lett. 145, 109–123.

Nimmo, F., Mckenzie, D., 1998. Volcanism and tectonics on Venus. Annu. Rev. Earth Planet. Sci. 26, 23–51.

O'Neill, C., Jellinek, A.M., Lenardic, A., 2007. Conditions for the onset of plate tectonics on terrestrial planets and moons. Earth Planet. Sci. Lett. 261, 20–32.

Orth, C.P., Solomatov, V.S., 2011. The isostatic stagnant lid approximation and global variations in the Venusian lithospheric thickness. Geochem. Geophys. Geosyst. 12, Q07018.

Pauer, M., Fleming, K., Čadek, O., 2006. Modeling the dynamic component of the geoid and topography of Venus. J. Geophys. Res. 111, E11012.

Rappaport, N.J., Konopliv, A.S., Kucinskas, A.B., 1999. An improved 360 degree and order model of Venus topography. Icarus 139, 19–31.

Reese, C.C., Solomatov, V.S., Baumgardner, J.R., Yang, W.S., 1999. Stagnant lid convection in a spherical shell. Phys. Earth Planet. Inter. 116, 1–7.

Richards, M.A., Yang, W.-S., Baumgardner, J.R., Bunge, H.-P., 2001. Role of a low-viscosity zone in stabilizing plate tectonics: implications for comparative terrestrial planetology. Geochem. Geophys. Geosyst. 2, 2000GC000115.

Roberts, J.H., Zhong, S., 2006. Degree-1 convection in the Martian mantle and the origin of the hemispheric dichotomy. J. Geophys. Res. 111, E06013.

Schubert, G., Solomatov, V.S., Tackley, P.J., Turcotte, D.L., 1997. Mantle convection and the thermal evolution of Venus. In: Bougher, S.W., Hunten, D.M., Philips, R.J. (Eds.), Venus II: Geology, Geophysics, Atmosphere, and Solar Wind Environment. University of Arizona Press, Tucson, pp. 1245–1288.

Simons, M., Solomon, S.C., Hager, B.H., 1997. Localization of gravity and topography: constraints on the tectonics and mantle dynamics of Venus. Geophys. J. Int. 131, 14–44.

Sjogren, W.L., Banerdt, W.B., Chodas, P.W., Konopliv, A.S., Balmino, G., Barriot, J.P., Arkani-Hamed, J., Colvin, T.R., Davies, M.E., 1997. The Venus gravity field and other geodetic parameters. In: Bougher, S.W., Hunten, D.M., Philips, R.J. (Eds.), Venus II: Geology, Geophysics, Atmosphere, and Solar Wind Environment. University of Arizona Press, Tucson, pp. 1125–1161.

Smrekar, S.E., Elkins-Tanton, L., Leitner, J.J., Lenardic, A., Mackwell, S., Moresi, L., Sotin, C., Stofan, E.R., 2007. Tectonic and thermal evolution of Venus and the role of volatiles: implications for understanding the terrestrial planets. In: Esposito, L.W., Stofan, E.R., Cravens, T.E. (Eds.), Geophysical Monograph. American Geophysical Union, Washington, DC, pp. 45–71.

Smrekar, S.E., Parmentier, E.M., 1996. The interaction of mantle plumes with surface thermal and chemical boundary layers: applications to hotspots on Venus. J. Geophys. Res. 101, 5397–5410.

Smrekar, S.E., Phillips, R.J., 1991. Venusian highlands: geoid to topography ratios and their implications. Earth Planet. Sci. Lett. 107, 582–597.

Smrekar, S.E., Sotin, C., 2012. Constraints on mantle plumes on Venus: implications for volatile history. Icarus 217, 510–523.

Smrekar, S.E., Stofan, E.R., Mueller, N., Treiman, A., Elkins-Tanton, L., Helbert, J., Piccioni, G., Drossart, P., 2010. Recent hotspot volcanism on Venus from VIRTIS emissivity data. Science 328, 605–608.

Steinbach, V., Yuen, D.A., 1992. The effects of multiple phase-transitions on Venusian mantle convection. Geophys. Res. Lett. 19, 2243–2246.

Stofan, E.R., Smrekar, S.E., Bindschadler, D.L., Senske, D.A., 1995. Large topographic rises on Venus: implications for mantle upwelling. J. Geophys. Res. 100, 23317–23327.

Tackley, P.J., 1996. On the ability of phase transitions and viscosity layering to induce long wavelength heterogeneity in the mantle. Geophys. Res. Lett. 23, 1985–1988.

Tackley, P.J., Stevenson, D.J., Glatzmaier, G.A., Schubert, G., 1993. Effects of an endothermic phase-transition at 670 km depth in a spherical model of convection in the Earths mantle. Nature 361, 699–704.

Tackley, P.J., Stevenson, D.J., Glatzmaier, G.A., Schubert, G., 1994. Effects of multiple phase-transitions in a 3-dimensional spherical model of convection in Earth's mantle. J. Geophys. Res. 99, 15877–15901.

van Hunen, J., Zhong, S., Shapiro, N.M., Ritzwoller, M.H., 2005. New evidence for dislocaton creep from 3-D geodynamic modeling of the Pacific upper mantle structure. Earth Planet. Sci. Lett. 238, 146–155.

Zhong, S.J., 2006. Constraints on thermochemical convection of the mantle from plume heat flux, plume excess temperature, and upper mantle temperature. J. Geophys. Res. 111, B04409.

Zhong, S.J., Gurnis, M., 1994. Role of plates and temperature-dependent viscosity in phase-change dynamics. J. Geophys. Res. 99, 15903–15917.

Zhong, S.J., McNamara, A., Tan, E., Moresi, L., Gurnis, M., 2008. A benchmark study on mantle convection in a 3-D spherical shell using CitcomS. Geochem. Geophys. Geosyst. 9, Q10017.